The changing nature of Earth's reflected sunlight

Graeme L. Stephens, Maria Z. Hakuba, Seiji Kato, Andrew Gettelman, Jean-Louis Dufresne, Timothy Andrews, Jason N. S. Cole, Ulrika Willen, Thorsten Mauritsen

PROCEEDINGS OF
THE ROYAL SOCIETY A
MATHEMATICAL, PHYSICAL AND ENGINEERING SCIENCES

The changing nature of Earth's reflected sunlight

Journal:	*Proceedings A*
Manuscript ID	RSPA-2022-0053
Article Type:	Research
Date Submitted by the Author:	20-Jan-2022
Complete List of Authors:	Stephens, Graeme; Jet Propulsion Laboratory; Oxford University, Atmospheric and oceanic sciecne Kato, Seiji; NASA Langley Research Center, Climate Science Branch Gettleman, Andrew; Oxford University, Physics; NCAR, Dufresne, Jean-Louis; Institut Pierre et Simon Laplace Cole, Jason N.S.; Canadian Centre for Climate Modelling and Analysis Environment and Climate Change Canada Willem, Ulrika; Swedish Meteorological and Hydrological Institute Hakuba, Maria; NASA Jet Propulsion Laboratory Andrews, Timothy; Met Office Hadley Centre Mauritsen, Thorsten; Stockholm University, Department of Meteorology
Subject:	Atmospheric science < EARTH SCIENCES, Climatology < EARTH SCIENCES
Keywords:	Earth albedo, reflected sunlight, Earth's energy imbalance
Subject Category:	Earth Science

Author-supplied statements

Relevant information will appear here if provided.

Ethics

Does your article include research that required ethical approval or permits?:
This article does not present research with ethical considerations

Statement (if applicable):
CUST_IF_YES_ETHICS :No data available.

Data

It is a condition of publication that data, code and materials supporting your paper are made publicly available. Does your paper present new data?:
My paper has no data

Statement (if applicable):
CUST_IF_YES_DATA :No data available.

Conflict of interest

I/We declare we have no competing interests

Statement (if applicable):
CUST_STATE_CONFLICT :No data available.

The changing nature of Earth's reflected sunlight

Graeme L Stephens[1,2], Maria Z Hakuba[1], Seiji Kato[3], Andrew Gettleman[4], Jean-Louis Dufresne[5], Timothy Andrews[6], Jason N.S. Cole[7], Ulrika Willem[8], and Thorsten Mauritsen[9]

1. Jet Propulsion Laboratory, California Institute of Technology, Pasadena, CA
2. Department of Physics, University of Oxford
3. NASA Langley Research Center
4. National Center for Atmospheric Research, Boulder, CO, USA
5. Laboratoire de Meteorologie Dynamique, Institut Pierre et Simon Laplace, Paris, France
6. Met Office Hadley Centre, Exeter, UK
7. Canadian Centre for Climate Modelling and Analysis, Environment and Climate Change Canada, Victoria, BC, Canada
8. Rossby Centre, Swedish Meteorological and Hydrological Institute, Norrkoping, Sweden
9. Department of Meteorology, Stockholm University, Stockholm, Sweden

Abstract

The increased rate of sea level rise suggests that Earth's energy imbalance is also increasing over time, which is also supported by observations made by sensors flown on Earth orbiting satellites over the past two decades. This study assesses whether the modern satellite observations of this energy imbalance support a real trend and the components of that trend and finds the imbalance observed is consistent across multiple sources of observations. The majority of recent studies now clearly point to this energy imbalance being positive, while forced by increasing greenhouse gas concentrations in the atmosphere, is amplified significantly by decreases to the amount of sunlight reflected by Earth to space. Here we show that the global changes observed appear largely from reductions in the amount of sunlight scattered by Earth's atmosphere. These reductions, in turn, are found to be almost equally split between reduced reflection from the cloudy and clear regions of the atmosphere, with the latter being suggestive of reduced scattering by aerosol particles over the observational period. Climate models, however, show an almost exclusive response from clouds, and a slightly exaggerated darkening of the surface. Thus, models that match the global shortwave change do so for the wrong reasons.

1.0 Introduction

We generally think of Earth as the "blue planet", and sometimes refer to it as the ocean planet. The surface of Earth, after all, is approximately 70% covered by oceans that occupy approximately 97% of the Earth's habitable space, contains approximately 97%

of the water on the planet and stores enormous amounts of heat that modulates our climate. The oceans are also the principal source of the water that resides in the atmosphere which is only about 0.001% of the total water on Earth. This tiny amount of water, however, profoundly affects Earth's weather and climate and the portion of the habitable space on Earth occupied by humans. An even smaller fraction of the water in air (about 0.5% of the total atmospheric water content, e.g. Stevens and Bony, 2013; Stephens et al., 2020) exists in condensed form as cloud droplets, ice crystals, snow-flakes and rain. This minute amount of water is the pathway through which fresh water is delivered to our lakes and reservoirs, replenishes aquifers, fills our rivers and supports human life. This tiny amount of water is also spread across Earth as a thin, white reflecting veil covering approximately 74% of the Earth (e.g. Stubenrauch et al., 2013).

Given that Earth is largely a cloud covered planet reflecting sunlight to space with the further addition of reflection from areas of white snow and ice cover at the Earth's surface, Earth might appropriately be considered to be just as much a white planet as a blue planet. A measure of the whiteness of Earth is its albedo which is the fraction of the incoming solar energy scattered by Earth back to space. Today this fraction is about 29% (e.g. Stephens et al., 2012,2015) although Earth's albedo has changed over its history. Figure 1 offers a sense of potential range of such changes that have occurred over time. The figure highlights the bifurcation of Earth's global mean surface temperature as created from the zero-dimensional energy balance model of Earth discussed by Pierrehumbert et al (2011). Similar to but of different context to the study of Budyko (1969), this model predicts that a bifurcation of the mean surface temperature occurs as

atmospheric concentrations of CO_2 change expressed in the figure as the partial pressure of CO_2 (p CO2). Only a single snowball Earth climate-state can exist under the conditions of small values of pCO_2 or in Earth's early history when the Suns' illumination was less than today. Similarly, a single solution only exists when pCO2 is large being an ice-free state, perhaps exemplified in the Late Paleocene Thermal Maximum 55 Mya (e.g., Zachos et al., 2008). The intermediate- pCO2 solutions exist as multiple intermediate temperature states for any given pCO2 separating the attractor basin of the upper warm state from the lower snowball state. Under certain conditions, these intermediate states can be unstable whereby only small changes to pCO2 at the left or right boundaries of the hysteresis (dashed arrows) result in dramatic changes in the climate state of the planet.

The estimated range of Earth's albedo associated with this hysteresis cycle is indicated to the left of the Figure. We can surmise the global albedo in the Snowball Earth state would be of order 0.6 based on our current understanding of the albedo of land and sea ice although this value is subject to debate given the large range of ice albedo values we observe today (e.g. Gardner and Sharp, 2010). A value of 0.6 was also assumed by Pierrehumbert et al. (2011) in creating Figure 1 and is also consistent with the value used in other paleoclimate model studies such as that of Voigt and Marotzke, (2010). It can be reasonably argued that the albedo of a warm state exceeds the lower limit deduced from a present-day clear-sky Earth value of 0.149 because the Paleocene–Eocene Thermal Maximum was also a period of an active hydrological cycle with evidence of significant transports of moisture poleward (Pagini et al., 2006) suggesting a planet of significant cloudiness. In today's climate, reflection from Earth's clouds contributes about 50% of

the total sunlight reflected to space (e.g., Stephens et al., 2015) and thus the albedo of a warm state Earth could be expected to have a similar magnitude cloud contribution. The estimate of 0.275 for the albedo in these warm states is based on present-day observations with a contribution of low-lying marine clouds removed (refer to Appendix). The rationale for this omission rests with the idealized model study of Schneider et al. (2019) who speculate that these low clouds largely disappear under strong warming.

This discussion sets the context for the present study. The purpose of this paper is to document the degree of change to Earth's albedo that has been observed over the modern era of observations made by sensors flown on Earth orbiting satellites and indicate the source of this change. From the earliest satellite measurements, beginning with those of VonderHaar and Suomi (1971) to the measurements of today, these observations have revealed a remarkably small interannual variability, less than 0.7% of the annual mean reflected flux (Figure 2 and related discussion). This lack of variability has existed over a period of time when changes to reflecting surfaces have occurred by, for example, the systematic reduction of polar sea ice (e.g. Walsh et al., 2019) or seasonal snow over (e.g. Robinson, 2020). A few basic questions arise from the study of existing observations that are addressed. These include 1) to what extent is Earth's albedo buffered from these systematic and ongoing changes at the surface of Earth? 2) If some form of buffering exists what are the mechanisms by which Earth's albedo remains resistant to these changes? 3) If not these changes to Earth reflecting surface what then are the causes for any changes observed over the period studied? This study attempts to answer these questions and reveals the ways that the influence of changes to Earth's reflecting surfaces, for example, are dampened by the overlying atmosphere. We show how these

processes exert an overall dominant influence on the solar radiation reflected by Earth to space.

The paper begins with a short review of the almost 20 years of satellite observations of Earth's radiation balance. A description of an analysis method used to dissect the reflected solar radiation into its main components, following the approach introduced by Stephens et al (2015), is described in section 3. When applied to the approximate 20-year time series of flux observations, a number of important insights are then revealed about the longer term time changes that are described in sections 4 and 5. Comparison to CMIP6 AMIP model simulated time series for the same period are also analyzed and compared to the observations in section 6.

It is worth noting at this point that recent studies have applied the analysis method adopted in this study to the same data although with a different a focus than that of the present study. Loeb et al. (2019), for example, use the decomposition method to shed light on the sources intra- and inter-annual variability of observed fluxes whereas Jonsson and Bender (2021) use the method to examine variability in the symmetry of the hemispheric albedo observed over the period of the CERES data record.

2.0 Data Sources

Two main sources of data serve the analyses presented in this study. The first data type is the CERES Energy Balance and Filled (EBAF) Ed. 4.1 top-of-atmosphere (TOA) flux product (Loeb et al. 2018) with matching surface radiative flux data (Kato et al., 2018).

These matched fluxes are made from a combination of observations and radiative transfer calculations archived in the form of monthly means for March 2000–March 2020 set on a 1°X1° latitude-longitude grid.

The second main source of data comes from the Coupled Model Intercomparison Project Phase 6 (CMIP6; Eyring et al., 2016). The simulations analyzed are forced with monthly time-varying observationally derived fields of SST and SIC using the Atmospheric Model Intercomparison Project (AMIP) boundary conditions (Gates et al., 1999; Hurrell et al., 2008; Taylor et al., 2000). As in the study of Loeb et al. (2020) the simulations were extended beyond the official end-date of CMIP6 AMIP in 2014 through the end of 2017. Six model groups provided these AMIP time series of fluxes both at the TOA and surface that can be compared to the CERES data. For the AMIP simulations, atmospheric composition is held fixed at their 2014 levels between 2015-2017 for all models except EC-Earth3-Veg, which used the Shared Socioeconomic Pathways (SSP2-4.5) greenhouse gas and aerosol concentrations (Riahi et al., 2017). The simulations are forced with monthly time-varying observationally derived fields of sea surface temperature (SST) and sea ice concentration (SIC) from either the merged Reynolds/HadISST1 (Hurrell et al., 2008) or the HadISST1 dataset (Rayner et al. 2003) only as described in Loeb et al. (2020).

We also use a third source of data products in this study. The CERES TOA flux product partitioned by cloud type (Edition 4A FluxByCloudType, Sun et al., 2021) is used to define the contribution of low marine clouds to TOA flux changes as described in

Appendix A. This contribution was extracted from the observed TOA fluxes to obtain the albedo value of 0.275 cited above to represent a climate state without these low marine clouds.

Figure 2 summarizes the CERES TOA flux data time series analyzed in this study and offers some context for considering the changes to Earth's reflected solar radiation described below. The figure presents the de-seasonalized monthly anomaly, global mean time series of TOA outgoing longwave flux, reflected shortwave flux and the net TOA flux, hereafter the Earth's energy imbalance (EEI). These anomalies are defined as the deviation of monthly mean flux from respective climatological monthly means where the latter are computed by averaging each month individually over the 20-year record. Positive anomalies represent an anomalous increase of energy input to Earth and negative anomalies imply periods of enhanced energy that escapes to space. Also included on the Figure as grey shading is the multivariate ENSO index (https://psl.noaa.gov/enso/mei/, Wolter et al., 2011, Zhang et al., 2019) provided for reference only and merely serves as a reminder of the principal role of ENSO in shaping the interanual variations in TOA fluxes observed. The estimated linear trends, a focus of this study, and a measure of the interannual variability quantified as the standard deviation of the detrended and de-seasonalized monthly reflected flux anomalies are also provided. The statistical significance of the trends is addressed below. The standard deviations reveal a remarkable lack of interannual variability in the SW reflected flux and thus also in the Earth's Albedo (e.g., Kato, 2009; Stephens et al., 2015) when compared to the magnitude of the global mean reflected flux itself which is about 100 Wm^{-2}.

A number of questions can be raised in relation to the interannual variability and trends revealed in Figure 2. Although it has been argued that the precision of the data exceeds the radiometric accuracy, the intrinsic measurement uncertainties associated with the individual longwave (LW) and shortwave (SW) components are larger than either the interannual variations observed or the estimated linear trends detected and thus questions about the realism of these changes can be legitimately raised. Despite these issues, there are a number of reasons why the observed changes are taken to be real in the present study: 1) the variability and trend in net TOA flux is also largely reproduced in independent estimates of the EEI such as derived from combinations of altimetric and gravimetric observations of GRACE that provide estimates of the total ocean heat uptake (e.g., Hakuba et al., (2021) in contrast to the Ocean heat uptake data used in Loeb et al., (2021a), 2) the trend in the net shortwave, the dominant source of the trend in the net flux, is also broadly supported in the analysis of measurements of Earth shine over a similar period of time (e.g., Goode et al. 2021) although with a smaller amplitude than that of Figure 2, 3) much of the behavior of the observed multi-annual changes evident in the EBAF data record shown in Figure 2 can be reconstructed from multiple independent observational data records applied to radiation kernels (e.g., Kramer et al. 2021) and 4) historical EEI simulations from climate models resemble the observed record (Loeb et al. 2020) and can only be reproduced using known radiative forcings (Raghuraman et al. 2021; also Kramer et al. 2021). Although these threads of evidence collectively support the credibility of the observed EBAF record, further scrutiny of the observational trends is still required.

3.0 The component analysis of Earth's reflected energy

The main components of Earth's reflected sunlight are analyzed in this study using the simple radiative transfer model of Stephens et al. (2015) that has a number of similarities to that introduced earlier by Donohoe and Battisti (2011). Figure 3 represents a simple model of reflection by a single homogenous, absorbing-scattering layer of atmosphere overlying a reflecting surface. For our purposes, the (hemispheric) solar radiative fluxes in and out at the top and bottom of the atmosphere are taken to be known from CERES EBAF observations and equivalently from the model simulations. These boundary fluxes then define the following system quantities:

The system reflectance (=albedo): $R = F_{TOA} / S$ (1)

The system transmittance $T = F_S / S$ (2)

where $S = F_{TOA}$ is the incoming solar flux at the TOA, $F^{\uparrow}_{TOA}$ is the reflected flux at the TOA and $F^{\downarrow}_{S}$ is the downward flux at the surface. The system absorption then follows as $A=1-R$. The objective is to examine the relation between the system properties A, R and T and the inherent atmospheric layer reflection and transmission properties we introduce here as r, t and the surface albedo

$$= F_S / F_S \qquad (3)$$

which then provides a way of associating the factors that influence r and t and the separate influence of α on these system properties R, T. The relationships between the fluxes at the boundaries of the atmosphere to the inherent properties of the atmosphere follow from application of the interaction principle [e.g., Flatau and Stephens, 1988]:

$$F_{TOA} = r_+ S + t_+ F_S \qquad (4a)$$
$$F_S = t\ S + r\ F_S \qquad (4b)$$

where the quantities $r_\pm$ and $t_\pm$ are the intrinsic reflection and transmission properties of the atmospheric layer and 1-r-t is the layer absorption, which differs from the system absorption A by the amplification effects of reflection and absorption of the surface on the latter. The ± sign refers to the polarity (direction) of the flow and typically $r_+ = r_-$ and $t_+ = t_-$ as now assumed with the "+" and "-" subscripts dropped. The combination of (4b) and (3) yields

$$T = \frac{F_S}{S} = \frac{t}{1\ \ r} \qquad (5a)$$
$$R = r + \frac{t\ \ t}{1\ \ r} \qquad (5b)$$

According to (5b) there are two main contributions to the system albedo – one contribution from atmospheric scattering r and now referred to as the atmospheric contribution and the second term being the surface contribution involving the multiple reflections between the surface and atmosphere and the attenuation by the atmosphere as this radiation propagates upward to space. Clouds are the dominant contribution to the atmospheric contribution through a combination of influences from macroscopic cloud properties including cloud amount and from intrinsic properties like cloud optical depth that define the albedo of clouds themselves [Stephens, 2005].

Since the system albedo R (defined at the TOA) , system transmission T, and the surface albedo α are known from the given boundary fluxes provided by CERES EBAF data record, then (5a) and (5b) can be inverted to express the intrinsic properties r, t in terms of these known system properties

$$t = T\frac{[1-\alpha R]}{1-\alpha^2 T^2} \qquad (6a)$$

$$r = R - t\alpha T \qquad (6b)$$

The main outputs of the model quantities examined are thus the albedo R (or equivalently the reflected flux SR), the atmospheric contribution to the albedo r, and the surface contribution ($t\alpha t/(1-r\alpha)$), and the product of these components with S, which define the respective flux contributions by the processes that define these terms.

4.0 Observed changes in the sunlight reflected by Earth

The analysis represented by (5) and (6) is applied to both the time series of CERES data and to the model output described in section 6 to quantify the different factors that contribute to the observed and modelled changes to solar radiation reflected by Earth such as shown in Figure 2a. The results of the analysis of observations are summarized in Figure 4 to Figure 8. Figure 4 provides insight on specific features of the analysis that are important for interpreting the results summarized in later figures. What is presented in Figure 4a and b are the ratios of the TOA flux contributions from the surface ($St\alpha t/(1-r\alpha)$) to the flux reflected from the surface $F_S^{\uparrow}$. This ratio is a bulk measure of the atmospheric transmission and thus a measure of the attenuation of surface fluxes by the atmosphere as the propogate to the TOA. Figures 4a and b present the global, annual mean distributions of this attenuation for both clear sky and all sky conditions respectively. For later reference, the trend in upwelling surface flux is also provided in Figure 4c. Two notable points about the maps of transmission require emphasis. The attenuation of surface reflected fluxes is largest in polar regions, that is where path

lengths are long and transmission is minimum, typically less than 0.4. Second, the clear sky transmission, as expected, is significantly larger over most the globe compared to transmission under all sky conditions and notably so where midlatitude cloud systems and Earth's storm track regions reside. This merely underscores the important role of clouds as a source of attenuation of surface flux changes.

Figures 5a and b present the trends of the different components of the TOA fluxes introduced above. Figure 5a provides the global-mean trends in the total observed top-of-atmosphere (TOA) reflected flux (*SR* and referred to as TOA all sky), the contribution to this flux by the all-sky reflection from the atmosphere (*Sr*, Atmos all) and from the surface ($St\alpha t/(1-r\alpha)$, Surface all) and then the respective contributions of the clear sky fluxes. Included on each histogram are the 95% confidence intervals derived using the t-test statistic that are used as a test of statistical significance of the trends. Figure 5b further breaks down the contributions to the atmospheric component including the cloud radiative effect being the difference between the all-sky and clear sky components. The colored bars convey information about the surface components discussed below.

A number of important observations emerge from the observed trends (Figure 5). First the results show that changes to surface reflection, dominated by changes to polar snow cover and sea ice, for example, have only a small influence on the observed global-mean TOA trend. The trend in the global-mean surface contribution is not significantly different from zero at the 95 percent level. By contrast, all trends of non-surface components are statistically significant at the 95% confidence level and the observed

trend in total reflected flux manifestly occurs as a result of changes to the reflection from Earth's atmosphere and not from the surface. As shown below, this change to atmospheric scattering is dominated by changes occurring in the low and mid-latitude atmosphere, a point also noted by Loeb et al. (2020). The second main result conveyed in Figure 5a, and one not commonly appreciated, is the contribution to the observed trend in the TOA flux by the atmosphere has a significant contribution that comes from changes in clear sky atmosphere scattering that have occurred over the past two decades. This is revealed more clearly in Figure 5b in which the contributions by the atmosphere are further dissected into its cloudy and clear sky components indicating that the reduction in shortwave reflection to space is caused almost equally by the two. Since changes to atmospheric clear sky scattering are dominated by aerosols, this result is suggestive of a reduction in the atmospheric aerosol particle concentration.

The colored bars in Figure 5b further elaborate on the results of Figure 4. Presented are the changes determined to occur in the reflected flux from the Earth's surface (Sfc flux up) in contrast to the surface contribution to the TOA flux (TOA SFC all sky, repeated from Figure 4b) and the ratio of these fluxes that represents a measure of the transmission of the surface flux through the atmosphere has changed over time, which is interpreted as the trend in the atmospheric transmission. In a global mean sense only about 10% of any surface signature change is transmitted to the TOA, such that influences of surface albedo changes on the TOA radiation balance are highly attenuated suggesting that the planetary albedo is buffered to some degree from changes that occur at the surface.

5.0 Regional patterns of change

The spatial character of the trends are portrayed in Figures 6, 7 and 8, beginning with trends in the hemispheric means (Figure 6), trends quantified for different latitude zones (Figure 7) and finally in the form of maps of trends (Figure 8). The stippling shown on these maps represents regions where trends are statistically significant at the 95% confidence level and the error bars in Figures 6 and 7 are the 95% confidence intervals as described above in relation to Figure 5.

On the hemispheric scale, and as also noted by Datseris and Stevens (2021), the total changes in reflected sunlight by the two hemispheres are practically the same (Figure 6a) at least to within the 95% confidence range. These hemispheric responses, however, arise from different combinations of the mechanisms that operate within each hemisphere. The SH, for example, experiences a larger reduction in the cloud reflection compared to the NH, whereas the NH experiences larger reductions due to the surface contribution, especially at higher latitudes (Figure 7). Within the atmosphere, the SW cloud radiative effect (SWCRE) changes in the SH are ostensibly matched in the NH by changes to the clear sky scattering that is discussed in more detail below.

When viewed in the zonal context of Figure 7, the differences in the changes that occur between hemispheres begins to emerge more clearly. For example, the trends that arise from changes to surface reflection are, by and large, not statistically significant in all zones except for the NH polar region represented by the latitudes 60-90N. Larger changes are also experienced in the 30-60N zone compared to the SH counterpart due in part to

the changes observed in clear sky scattering over the 20 years of observations.

A more granular depiction of these changes is provided in the maps of Figure 8. The stippling on these maps shows how the significance of the trends of cloudy sky fluxes, unlike the global, hemispheric and zonal averages, is limited to just a few regions, such as in the areas of low clouds in eastern Pacific and in some regions of deep convection. These maps reveal that (i) the patterns of trends in the all sky reflected flux (Figure 8a), although of limited significance, are essentially a repeat of the regional patterns of post-hiatus minus pre-hiatus SW flux differences reported in Loeb et al. (2020); (ii) the TOA pattern of change and the all sky atmosphere pattern of change are essentially identical which merely reinforces the results of Figures 5, 6 and 7 that the atmospheric contribution is dominant, and (iii) this latter pattern appears to be shaped by the pattern of change of the SWCRE in the tropical region which reflects shifts in convection associated with interannual modes of variability with increased cloudiness in the tropical eastern Pacific and reductions of subtropical low clouds (e.g. Loeb et al., 2020). Although the amplitude of the change to clear sky reflection is smaller than the comparative amplitudes associated with cloud changes, the pattern of clear sky variability is both more coherent and of wide spread significance and when averaged either zonally (Figure 7), over each hemisphere (Figure 6) or globally (Figure 5) reveals a statistically significant reduction in clear sky scattering that is more prevalent in the NH. The clear sky trends presented in Figure 8c exhibit wide-spread reductions in reflected SW fluxes over the oceans and pronounced reductions in the NH. These latter findings are consistent with Loeb et al. (2021b) who estimates a trend of 0.18 ± 0.17 Wm^{-2} $decade^{-1}$ in net TOA solar

radiation associated with changes in aerosol optical depth, largely in the NH over the period of the CERES data record. Although consistent with the finding of the present study, the trend found in Loeb et al. (2021b) is smaller than the clear sky trend in the atmospheric component of the TOA flux shown in Figures 5, 6 and 7. While other factors can also contribute to these clear sky changes, such as water vapor increases that have also occurred over the same period (e.g. Stephens et al. 2020), off line calculations (not shown) of the increased absorption by this water vapor increase indicates it is too small to explain the difference in magnitudes of the present study to that of Loeb et al. (2021b). This is also supported in the study of Andrews et al (2015) who find that temperature related SW clear sky changes, such as from water vapor, are similarly small contributing approximately the same as surface albedo feedbacks to SW radiation budget changes. By contrast, non temperature related influences, such as that of aerosol, on these trends is a topic of ongoing research by multiple groups.

6.0 Comparison to models

TOA and surface radiative fluxes from six of the seven models used in the Loeb et al. (2020) study were analyzed using the method described above. The Loeb et al. (2020) study concludes that the seven CMIP models produce a time variation of TOA flux that broadly tracks CERES changes over time, a point further underscored in Figure 9 although the quantitative details of the comparison reveal some differences that are now noted. Four of the six models produce statistically significant trends at the 95% confidence level and, except for CESM2, with magnitudes slightly smaller than that of CERES. Two models produce small, non-significant trends in the TOA reflected flux.

The component analysis introduced above using the TOA and surface fluxes applied to the four models that produce a statistically significant TOA shortwave flux trend is presented in Figure 10 in the same format as Figure 5a. This analysis reveals both similarities with the observations but also important differences between the modeled and observed changes. As noted in discussion of the observations presented in Figure 5, the results of the four models analyzed also indicate that surface changes contributions produce only a small contribution to the changes to global mean TOA SW fluxes with three models producing trends that are marginally larger, statistically, zero (e.g. Figure 10d). Also like the observations, the modelled changes to TOA SW fluxes are dominated by changes to scattering by the atmosphere (Figure 9 compared to Figure 10a). Differences from the observations however emerge regarding how these atmospheric influences arise. The changes that do occur in the model fluxes are a result primarily of changes to clouds (Figure 10c) with minor and largely insignificant changes to the clear sky scattering (Figure 10b) unlike that observed which occur almost equally from changes to clear and cloudy sky scattering. Both observations and models reveal, for example, large reductions in shortwave fluxes over the East-Pacific (EP) low-cloud regions evident in Figure 8 and as highlighted in Loeb et al. (2020) who argue that the models ability to represent changes in the relationship between global mean net TOA flux and surface temperature depends upon how well it represents shortwave flux changes in low-cloud regions although with a sensitivity to the SST changes of the Eastern Pacific that is weaker than observed. Where the present study differs is it indicates that models

do not reproduce the clear sky flux changes evident in the record with a presumably weaker aerosol influence than implied in the observations.

7.0 Summary and conclusions

The net absorption of solar energy by Earth appears to be increasing over time according to observations made by sensors flown on Earth orbiting satellites over the past two decades. Given that this is a profound observation, many recent studies have focused on the examination of the changing EEI (e.g. Loeb et al. 2021a; Kramer et al. 2021; Raghuraman et al. 2021). We have analyzed the modern satellite observations of the EEI from CERES and found them consistent with other independent information, and thus credible although work contines to support this conclusion.

Recent studies on the change in EEI all reveal that by far the largest contribution to the increase in net absorption of solar energy by the planet resides in the reductions that have occurred over the past two decades in the amount of solar radiation reflected to space by Earth. We cannot say if these changes are unprecedented given they are small within the context of the historical changes that must have occurred over Earth's history. Although small in that context, the changes are both statistically significant at the 95% confidence level and profound. The purpose of this paper is to document the nature of the changes that have occurred to Earth's albedo and identify sources of these changes. The study attempts to answer a few basic questions about Earth's albedo associated with the observed changes. An analysis method is used to dissect the reflected solar radiation into its main components, following the approach introduced by Stephens et al. (2015), in

order to address the questions posed. This method is applied to the approximate 20-year time series of flux observations of CERES as well as to CMIP6 AMIP model simulated time series for the same period for comparison.

The questions posed and the subsequent findings of this study are as follows:

1) *To what extent is Earth's albedo buffered from the systematic and ongoing changes that we have experienced at Earth's surface through secular changes to polar sea ice and snow cover, for example?* Our analysis shows that changes to surface reflection, dominated by changes to polar snow cover and sea ice have no statistically significant impact on the observed TOA global-mean trend but when considered regionally, such as illustrated in Figure 7a, the influences on the TOA reflection by changes to the reflecting surfaces in higher latitudes is significant. The TOA system albedo, on the global scale, appears to be highly buffered from the changes that are observed at the Earth's surface.

2) *If some form of buffering exists what are the mechanisms by which Earth albedo remains resistant to these changes?* Our analysis points to the ways that the influences of changes to Earth's reflecting surfaces, for example, are substantially reduced at the TOA by atmospheric radiative transfer processes which, it is shown, exert an overall dominant influence on the solar radiation reflected by Earth to space and on the changes that are observed. The surface signal is strongly attenuated by the atmosphere (Figure 4) and, from a global perspective, the influences of surface changes experienced in the NH (e.g. Figures 6 and 7) are offset by cloud changes in the SH.

3) *If not these changes to Earth reflecting surface what then are the principal causes for any changes observed over the period studied?* The decreasing trend of TOA solar

reflection manifestly occurs as a result of changes to the reflection from Earth's atmosphere and not from the surface with the former being dominated by changes occurring in the low and mid-latitude atmosphere. Furthermore, we find that the contribution to the observed downward trend in the TOA reflected flux by the atmosphere has a significant contribution that comes from changes in clear sky atmospheric scattering that have occurred over the past two decades. These changes appear to be largely a result of reduction to the aerosol particle concentration, particularly in the NH (e.g. Loeb et al., 2021b).

The method was also applied to TOA and surface radiative fluxes from six of the seven CMIP6 models that were used in AMIP style experiments and studied by Loeb et al (2020). Four of the six models produce statistically significant global trends that are similar to but smaller than that of CERES while another two models produce small non-significant trends in the TOA reflected flux. From further component analysis of these four models we find:

1) A positive trend in EEI like that observed and also reported in Loeb et al (2020). The negative trend in reflected sunlight is the dominant factor in this EEI increase. However, the decrease in reflected energy in 3 of the four models analyzed is about half that observed.
2) Like the observations, models also find surface contributions to the TOA trend to be small and, unlike the observations, three models produce changes that are marginally different from zero when aggregated globally.

3) The contribution by the atmosphere dominates both modelled and observed trends, but the modelled contribution by the atmosphere is about half that observed in three of the four models analyzed.
4) The contribution by cloud changes in both the four models and observations are similar, however, the atmospheric contribution from models is almost entirely from clouds whereas the observed changes are comprised almost equally from cloud and clear sky changes.
5) Thus, models that match the observed trend do so for the wrong reasons: a too small clear sky atmosphere contribution, combined with a too strong surface and cloudy sky contribution.

Appendix

The Clouds and the Earth's Radiant Energy System (CERES) project provides a Flux By Cloud Type (FBCT) product that stratifies radiative fluxes by cloud-type. The FBCT product provides 1° regional daily and monthly shortwave (SW) and longwave (LW) cloud-type fluxes and cloud properties sorted by 7 pressure layers and 6 optical depth bins according to the ISCCP DX cloud-type definitions in Rossow and Schiffer (1991). Biases in the fluxes partitioned in this way are mitigated by constraining the cloud-type fluxes within each footprint with the CERES Single Scanner Footprint (SSF) observed flux. The FBCT all-sky and clear-sky monthly averaged fluxes were found to be consistent with the CERES SSF1deg product. The contribution by tropical and subtropical clow clouds used to deduce the 'warm state' albedo of Fig 1 was calculated by first aggregating the SW flux contributions from the FBCT product for all clouds below 680 hPa between 30N and S and the subtracting this area-weighted contribution from the total global reflected flux.

Acknowledgements
This work was funded in part by the Libera project under NASA Contract 80LARC20D0006

References

Andrews, T., J.M. Gregory and M.J.Webb, 2015; The Dependence of Radiative Forcing and Feedback on Evolving Patterns of Surface Temperature Change in Climate Models, J. Climate, 28, 1630–1648 ,https://doi.org/10.1175/JCLI-D-14-00545.1

Budyko, M.I., 1969; The effect of solar radiation variations on the climate of the Earth, *Tellus,* 21,DOI/10.1111/j.2153-3490.1969.tb00466.x

Datseris, G., & Stevens, B. (2021). Earth's albedo and its symmetry. *AGU Advances*, *2*, e2021AV000440. https:// doi.org/10.1029/2021AV000440

Donohoe, A and D.S. Battisti, 2011; Atmospheric and Surface Contributions to Planetary Albedo; *J. Climate*, 24, 4402–4418, DOI: https://doi.org/10.1175/2011JCLI3946.1

Eyring, V., Bony, S., Meehl, G. A., Senior, C. A., Stevens, B., Stouffer, R. J., & Taylor, K. E. (2016). Overview of the Coupled Model Intercomparison Project Phase 6 (CMIP6) experimental design and organization. *Geoscientific Model Development, 9, 1937–1958. https://* doi.org/10.5194/gmd-9-1937-2016

Flatau, P.J. and G.L. Stephens, 1988: On the Fundamental Solution of the Radiative Transfer Equation. *J. Geophys. Res*., **93**(D9**)**, 11,037-11,050.

Gardner, A. S., and M. J. Sharp (2010), A review of snow and ice albedo and the development of a new physically based broadband albedo parameterization, J. Geophys. Res., 115, F01009, doi:10.1029/2009JF001444.

Gates, W. L., Boyle, J. S., Covey, C., Dease, C. G., Doutriaux, C. M., Drach, R. S., et al., 1999; An overview of the results of the Atmospheric Model Intercomparison Project (AMIP I). *Bull. Amer. Meteorol. Soc*., 80(1), 29–55.https://doi.org/10.1175/1520-0477(1999)080<0029:AOOTRO>2.0.CO;2

Goode, P. R., Pallé, E., Shoumko, A., Shoumko, S., Montañes-Rodriguez, P., & Koonin, S. E. (2021). Earth's albedo 1998–2017 as measured from earthshine. *Geophy. Res. Lett*, 48, e2021GL094888. https://doi.org/10.1029/2021GL094888

Hakuba, M. Z., Frederikse, T., & Landerer, F. W. (2021). Earth's energy imbalance from the ocean perspective (2005–2019). *Geophysical Research Letters*, 48, e2021GL093624. https://doi.org/10.1029/2021GL093624

Hurrell, J., Hack, J., Shea, D., Caron, J., & Rosinski, J.,2008; A new sea surface temperature and sea ice boundary dataset for the community atmosphere model. *J. Climate*, 21. 5145–5153. https://doi.org/10.1175/2008JCLI2292.1

Jonsson, A and F.A-M Bender, 2021; Persitence and variability of Earth's inter-hemispheric albedo symmetry in 19 years of CERES EBAF observations, *J Climate*, DOI 10.1175/JCLI-D-20-0970.1.

Kato, S. (2009), Interannual variability of global radiation budget, *J. Clim*., 22, 4893–4907.

Kato, S. et al. ,2018; Surface Irradiances of Edition 4.0 Clouds and the Earth's Radiant Energy System (CERES) Energy Balanced and Filled (EBAF) Data Product. *J. Climate* 31, 4501– 4527

Kramer, R. J., He, H., Soden, B. J., Oreopoulos, L., Myhre, G., Forster, P. M., & Smith, C. J. (2021). Observational evidence of increasing global radiative forcing. *Geophys Res. Lett*, 48, e2020GL091585. https://doi.org/10.1029/2020GL091585

Loeb, N. G., and Coauthors, 2018: Clouds and the Earth's Radiant Energy System (CERES) Energy Balanced and Filled (EBAF) Top-of-Atmosphere (TOA) Edition 4.0 Data Product. *J. Climate*, doi:10.1175/jcli-d-17-0208.1.

Loeb, N.G., H. Wang, F.G.Rose, S. Kato,W.Smith Jr, and S.Sun-Mack, 2019; Decomposing Shortwave Top-of-Atmosphere and Surface Radiative Flux Variations in Terms of Surface and Atmospheric Contributions, *J.Climate*, 32, 5003-5019, DOI: 10.1175/JCLI-D-18-0826.1

Loeb, N. G., Wang, H., Allan, R. Andrews T., Armour, K., Cole, J. N. S., et al., 2020; New generation of climate models track recent unprecedented changes in Earth's radiation budget observed by CERES. *Geophys. Res. Letters*, 47, e2019GL086705. https://doi.org/10.1029/2019GL086705

Loeb, N. G., Johnson, G. C., Thorsen, T. J., Lyman, J. M., Rose, F. G., & Kato, S. ,2021a; Satellite and ocean data reveal marked increase in Earth's heating rate. *Geophys. Res. Lett*., 48, e2021GL093047. https://doi.org/10.1029/2021GL093047

Loeb, N. G., Su, W., Bellouin, N., & Ming, Y. ,2021b; Changes in clear-sky shortwave aerosol direct radiative effects since 2002. *J Geophys. Res: Atmos*, 126, e2020JD034090. https://doi.org/10.1029/2020JD034090

Pagani, M., Pedentchouk, N., Huber, M. *et al.*, 2006; Arctic hydrology during global warming at the Palaeocene/Eocene thermal maximum. *Nature* **442,** 671–675. https://doi.org/10.1038/nature05043

Pierrehumbert, R.T., D.S.Abbott, A. Voigt and D. Koll, 2011; Climate of the Neoproterozoic, *Annu. Rev. Earth Planet. Sci*. 2011.39:417-460

Raghuraman S.P., D.Paynter and V. Ramaswamy, 2021; Anthropogenic forcing and response yield observed positive trend in Earth's energy imbalance, *Nature Comms*., 12:4577, https://doi.org/10.1038/s41467-021-24544-4.

Rayner, N. A., D. E. Parker, E. B. Horton, C. K. Folland, L. V. Alexander, D. P. Rowell, E. C. Kent, and A. Kaplan, 2003; Global analyses of sea surface temperature, sea ice, and night

marine air temperature since the late nineteenth century, *J. Geophys. Res*.,108(D14), 4407, doi:10.1029/2002JD002670.

Riahi, K., et al. ,2017: The Shared Socioeconomic Pathways and their energy, land use, and greenhouse gas emissions implications: An overview. *Global Environ. Change*, 42, 153-168.

Richardson, M. T. (2022). Prospects for detecting accelerated global warming. *Geophys. Res. Lett*., 49, e2021GL095782. https://doi.org/10.1029/2021GL095782

Robinson, D.A., 2020; Northern Hemisphere continental snow cover extent [in Blunden, J. and D. S. Arndt, Eds., 2020: *State of the Climate in 2019*. Bull. Amer. Meteor. Soc., 101 (8), Si–S429 https://doi.org/10.1175/2020BAMSStateoftheClimate.1

Rossow, W.B., and R.A. Schiffer, 1991; ISCCP cloud data products, *Bull. Amer. Meteor. Soc*., 72, 654 2-20.

Schneider, T., C. M. Kaul and K. G. Pressel, 2019; Possible climate transitions from breakup of stratocumulus decks under greenhouse warming; *Nat. Geosci.,* doi.org/10.1038/s41561-019-0310-1

Stephens, G.L., 2005; Cloud Feedbacks in the Climate System: A Critical Review. *J. Clim.*, **18**, 237-273.

Stephens, G.L, J Li, Wild, C A Clayson, N Loeb, S. Kato, T L'Ecuyer, P W. Stackhouse Jr, and T Andrews, 2012; An update on Earth's energy balance in light of the latest global observations, *Nature Geosci.,5,*691-696

Stephens, G. L., D. O'Brien, P. J. Webster,P. Pilewski, S. Kato, and J.-l. Li, 2015; The albedo of Earth, *Rev.Geophys*., 53, doi:10.1002/2014RG000449.

Stephens, G.L., J..Slingo, J.T. Reager, P.Durack, M. Hakuba and J. Worden, 2020; Earth's water reservoirs in a changing climate, *Proc. Roy. Soc. (A)*, http://dx.doi.org/10.1098/rspa.2019.0458

Stevens, B and S. Bony, 2013; Water in the atmosphere, *Physics Today,* **66**, 6, 29; https://doi.org/10.1063/PT.3.2009

Stubenrauch, C. J., et al. , 2013; Assessment of global cloud datasets from satellites: Project and database initiated by the GEWEX radiation panel, *Bull. Am. Meteorol. Soc*., 94, 1031–1049, doi:10.1175/BAMS-D-12-00117.1.

Sun M., D.R. Doelling, N. G. Loeb, R. C. Scott, J. Wilkins,L. T. Nguyen, and P. Mlynczak, 2021; Clouds and the Earth's Radiant Energy System (CERES) FluxByCldTyp Edition 4 Data Product, *J. Atmos. and Oceanic Tech*. (in review)

Taylor, K. E., Williamson, D., & Zwiers, F.,2000; The sea surface temperature and sea ice concentration boundary conditions for AMIP II simulations, PCMDI Report No. 578 60, Program for Climate Model Diagnosis and Intercomparison, Lawrence Livermore National Laboratory.

Voigt A. and J. Marotzke, 2010; The transition from present-day climate to a modern Snowball Earth, *Clim Dyn*., DOI:10.1007/s00382-009-0633-5

Vonder Haar, T. H., and V. Suomi, 1971; Measurements of the Earth's radiation budget from satellites during a 5 year period. Part I: Extended time and space means, *J. Atmos. Sci*., 28, 305–314.

Walsh, J. E., W. L. Chapman, F. Fetterer, and J. S. Stewart, 2019: Gridded monthly sea ice extent and concentration, 1850 onward, version 2. NSIDC, accessed 1 November 2019, https://doi.org/10.7265/jj4s-tq79.

Wolter, K., and M. S. Timlin, 2011: El Niño/Southern Oscillation behaviour since 1871 as diagnosed in an extended multivariate ENSO index (MEI.ext).*Intl. J. Climatology*, **31**, 14pp., 1074-1087. DOI: 10.1002/joc.2336.

Zachos, J., Dickens, G. & Zeebe, R. An early Cenozoic perspective on greenhouse warming and carbon-cycle dynamics. *Nature* **451,** 279–283 (2008). https://doi.org/10.1038/nature06588

Zhang, T, A. Hoell, J. Perlwitz, J. Eischeid, D. Murray, M. Hoerling and T. Hamill, 2019: Towards Probabilistic Multivariate ENSO Monitoring, *Geophys. Res. Lett.*, **46**, DOI: 10.1029/2019GL083946

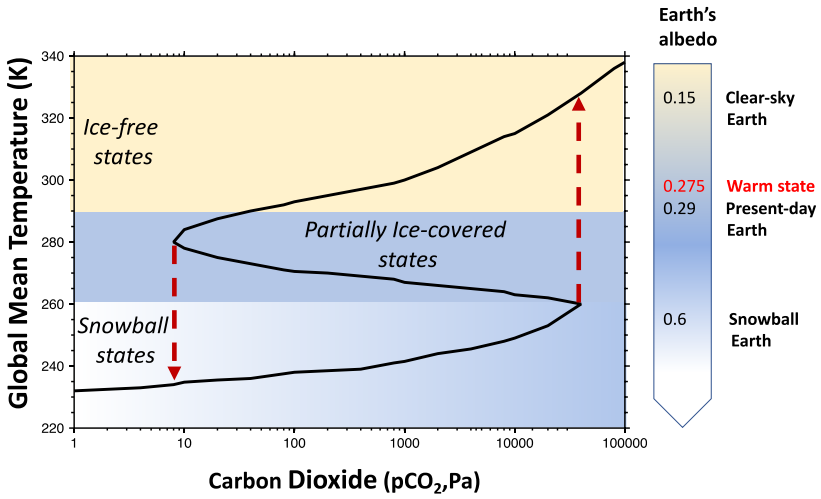

Figure 1: Bifurcation diagram derived from a zero-dimensional energy balance model by Pierrehumbert et al. (2011). Calculations performed assuming a value for ice albedo of 0.6. indicated in the key. pCO2 up to approximately 1,000 Pa, the inventory can be converted to a mixing ratio in parts per million by volume (ppmv) by multiplying by 6.6. The values listed to the right of the figure are estimates of the planetary albedo as described on text and as they align with surface temperature.

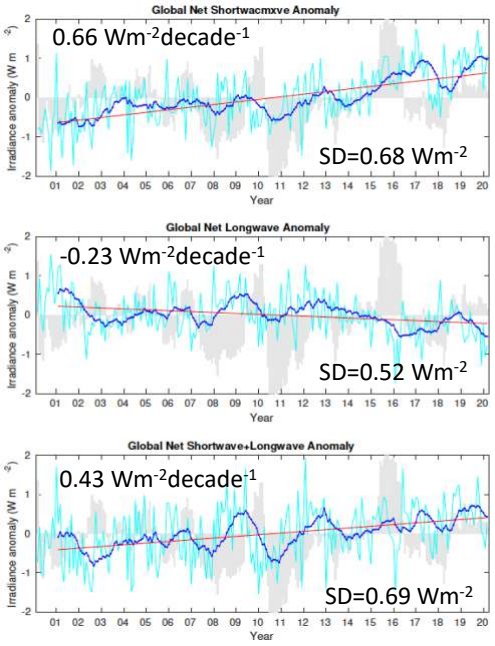

Figure 2: De-seasonalized monthly anomaly time series of top-of-atmosphere (TOA) net shortwave+longwave (total, lower panel, also referred to as the Earth's Energy Imbalance, EEI), net shortwave (upper panel), and net longwave fluxes (middle panel). A positive net flux represents an increase energy input to Earth. The blue line is computed with a 12-month running and the cyan lines is the raw monthly mean EBAF data. The red line in each panel is a linear regression of the smoothed time series.

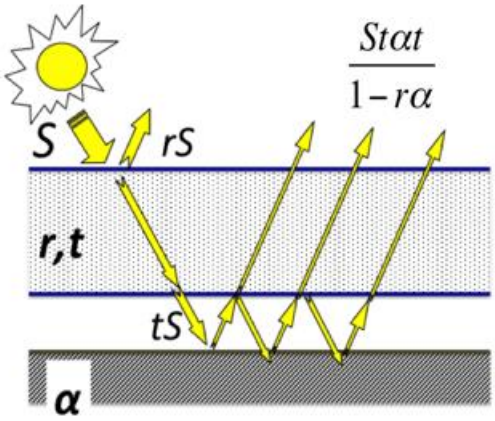

Figure 3 Schematic of a reflecting system composed of a single scattering and absorbing layer of atmosphere over a reflecting surface of albedo α and illuminated by a flux S. The intrinsic scattering properties of the atmosphere are governed by the reflectance r and transmittance t. The total reflectance of the system (system albedo) is given by (6b) and includes the reflected energy from the layer rS plus the multiple scattering between the surface and atmosphere (from Stephens et al., 2015).

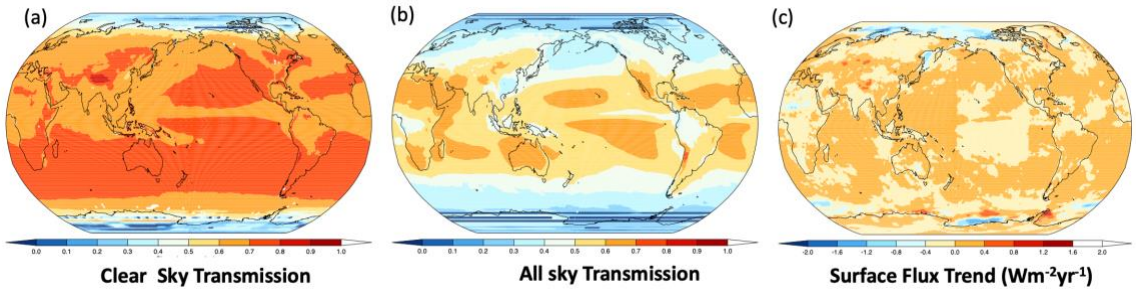

Figure 4 (a) The annual mean clear sky transmission that characterizes the SW flux reflected by the surface reaching the TOA; (b) as in (a) but the transmission of the cloudy and clear sky; (c) The trend in reflected SW flux from the surface (and determined at the surface).

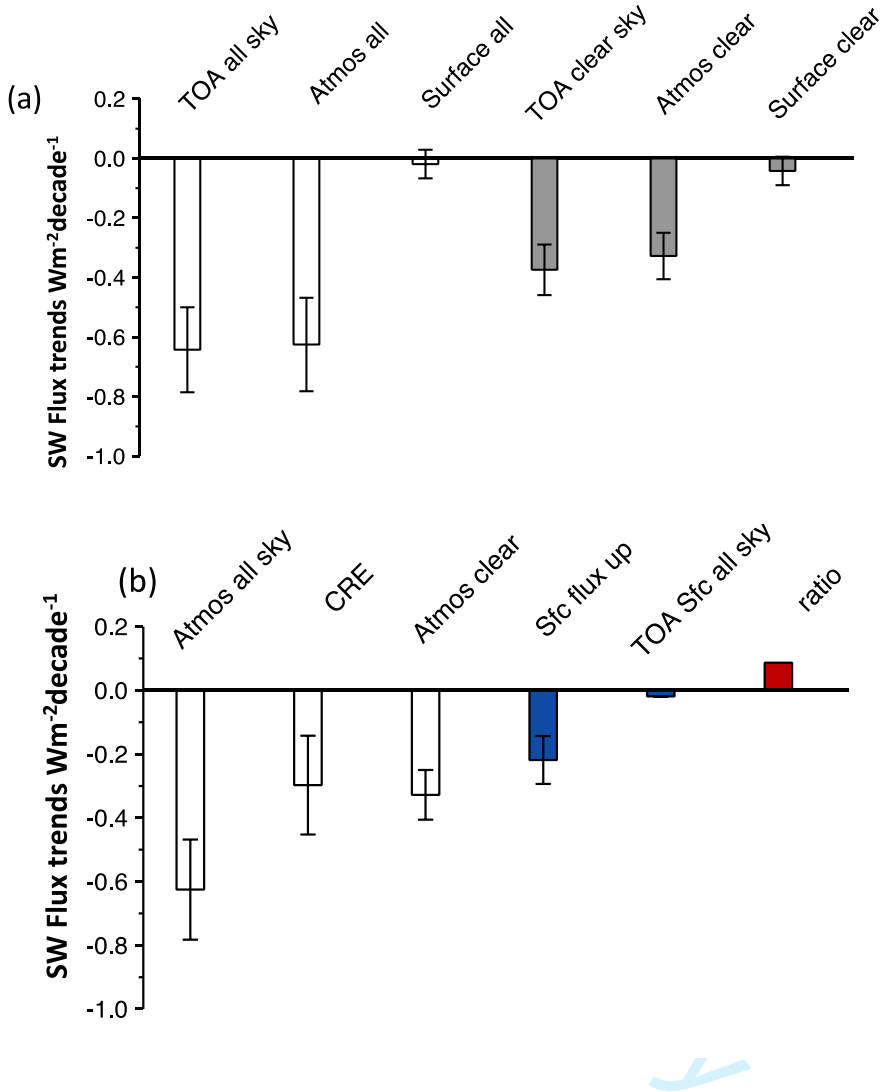

Figure 5 (a) Global-mean trends in total reflected solar radiation from Earth (TOA all-sky) and the contributions to it from the atmosphere (Atmos all) and surface (Surface all). Also shown are the respective clear sky components. Also shown are the 95% confidence intervals such that if this interval range includes zero then the trend is deemed not significantly different than zero. (b) Further decomposition of 1) the atmospheric component into the specific contribution by clouds (CRE) and by the clear sky atmosphere (Atmos clear) and 2) the surface contribution (TOA Sfc all sky) contrasted against the change in surface upward flux and the ratio of the two being an indicator of the attenuation by the atmosphere (refer to text).

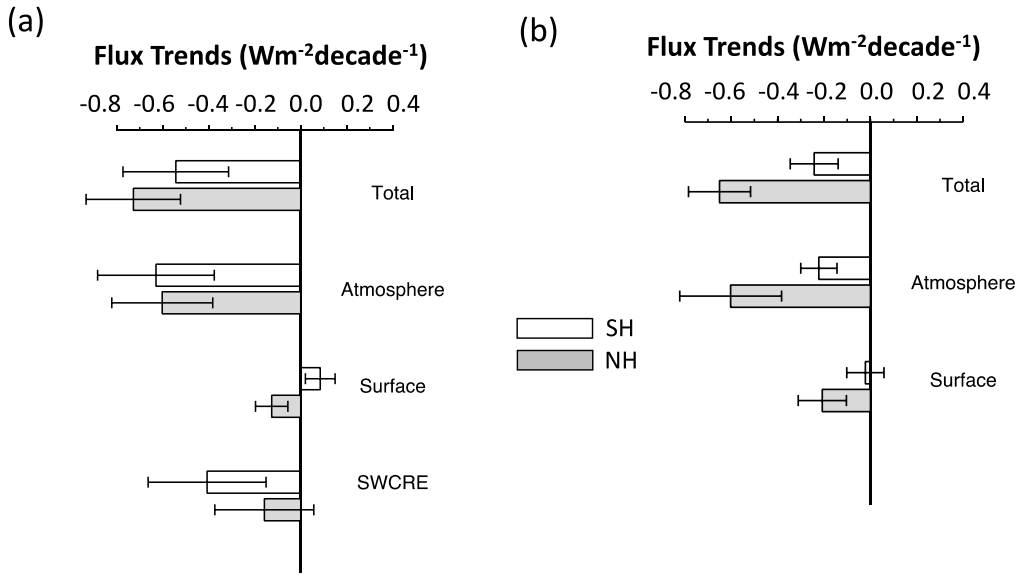

Figure 6 The hemispheric trends in the components of the TOA reflected solar radiation for (a) all-sky and (b) clear sky along the 95% confidence interval for each flux component.

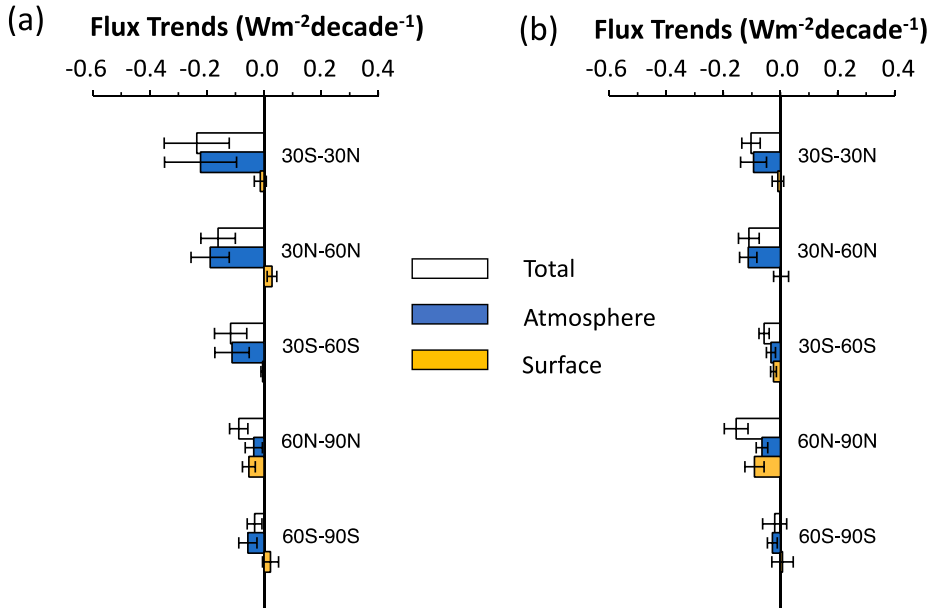

Figure 7 The trends in the components of the TOA SW flux broken down by latitude zone for (a) all-sky and (b) clear sky. Included are the 95% confidence intervals for each flux component. Each zone is fractionally weighted by area such that the global mean trend is the sum of the zones.

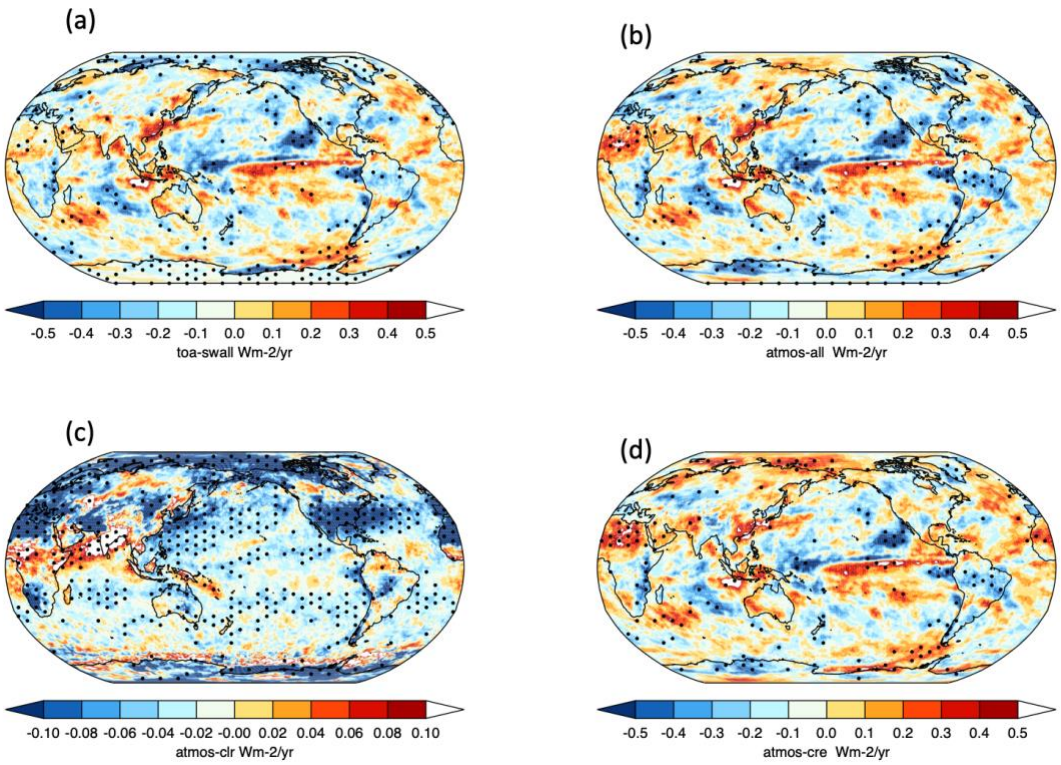

Figure 8 Global distributions of the trends in (a) total reflected sunlight by Earth, (b) the all-sky atmospheric component, (c) the clear sky component and (d) cloud radiative effects that sum to define the all sky component (a). The stippling represents those regions where trends are significantly different than zero at the 95% level.

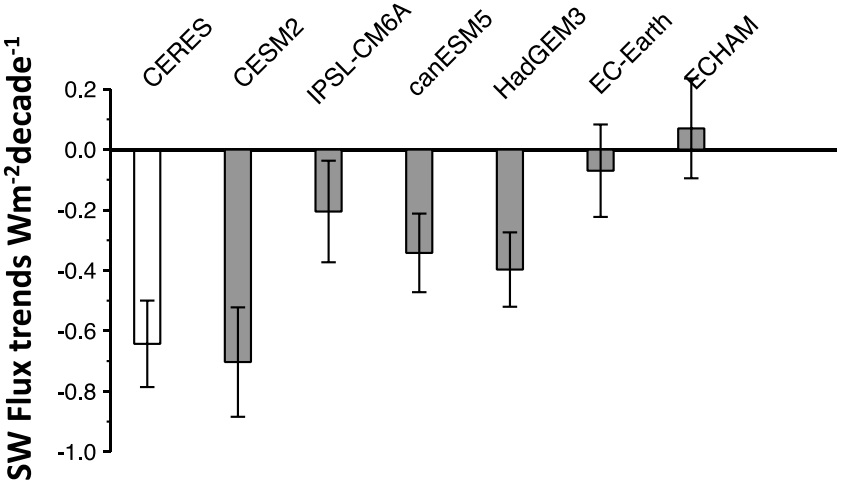

Figure 9 The all-sky TOA tends in global-mean reflected sunlight from CERES (reproduced from Figure 5a) and from 6 models highlighted. The 95% confidence interval is also provided for reference.

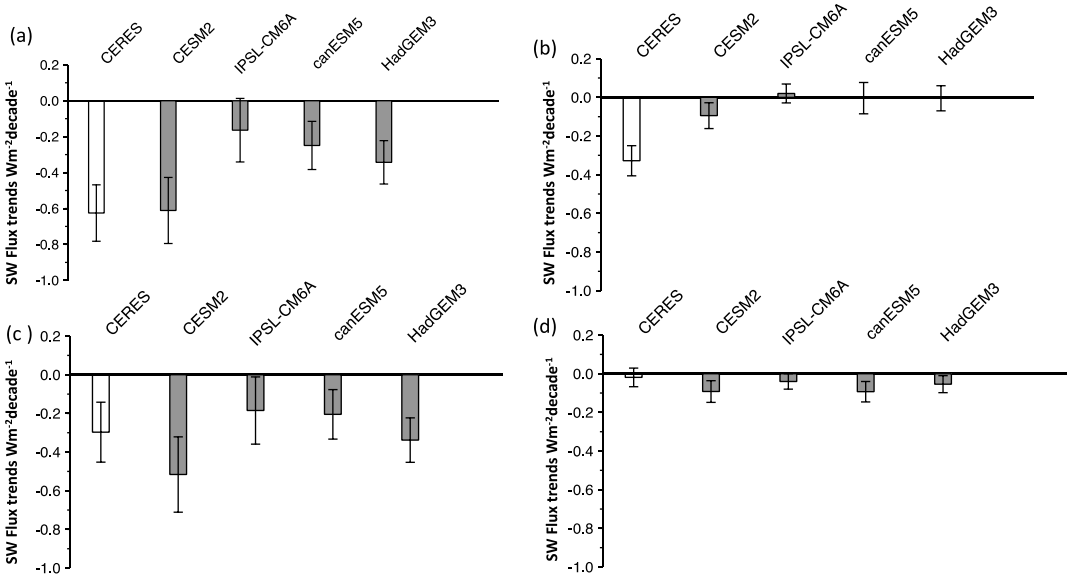

Figure 10 The shortwave reflected flux component trend analysis comparing CERES to that of 4 models. a) All sky atmospheric contribution, b) Clear-sky atmospheric contribution, c) The trend in the SWCRE and d) contribution to TOA changes by the surface changes